J. Phys. B: At. Mol. Opt. Phys. **40** (2007) 2969–2993 doi:10.1088/0953-4075/40/15/001

R-matrix electron-impact excitation calculations along the F-like iso-electronic sequence

M C Witthoeft, A D Whiteford and N R Badnell

Department of Physics, University of Strathclyde, Glasgow, G4 0NG, UK

Received 2 May 2007, in final form 11 June 2007
Published 13 July 2007
Online at stacks.iop.org/JPhysB/40/2969

Abstract

We present results for the electron-impact excitation of F-like ions from Ne^{+} to Kr^{27+} using an *R*-matrix approach where the intermediate-coupling frame transformation method has been used to obtain level-resolved collision strengths. For each calculation, the target has been expanded using 87 terms (195 levels) with the following configuration basis: $2s^2\ 2p^5$, $2s\ 2p^6$, $2s^2\ 2p^4\ 3l$, $2s\ 2p^5\ 3l$ and $2s^2\ 2p^4\ 4l$. Comparisons are made with previous *R*-matrix calculations for the fine-structure transition over the whole sequence and other, more extensive, calculations on Ne^{+} and Fe^{17+}. We examine iso-electronic trends of both low- and high-temperature effective collision strengths. This complete, self-consistent set of radiative and collision data is archived in multiple databases.

1. Introduction

For many years, *R*-matrix theory has been used successfully in performing large-scale calculations for the electron-impact excitation of atoms and ions. The *R*-matrix codes have continually evolved in step with the advances of computer technology. The most significant advance, in recent years, has been the increasing availability of parallel computers. Following the parallelization of the outer-region code by Gorczyca *et al* (1995) and the diagonalization of the inner region Hamiltonian by Mitnik *et al* (1999), the current suite of *R*-matrix codes[1] is now almost fully parallelized. An example of a recent calculation which takes full advantage of state-of-the-art parallel computers is the *R*-matrix with pseudostates calculation of electron-impact excitation of neutral Ne by Ballance and Griffin (2004) where hundreds of processors were used to perform the calculation. These types of calculations are necessary for such complex systems in order to describe the scattering target as accurately as possible. Since *R*-matrix calculations are so computationally intensive, only ions of particular importance are typically studied. Most of the calculations have been focused on the lighter elements up to Ne. Of the heavier elements, Fe is often studied because of its astrophysical importance. A

[1] The codes used for these calculations can be obtained at http://amdpp.phys.strath.ac.uk/tamoc/code.html.

good example of this can be seen in the publications from the IRON Project (see Hummer *et al* (1993)) where the focus is on the ion stages of iron.

Due to the continued advances in computer technology and the *R*-matrix codes themselves, it is now feasible to perform high-quality *R*-matrix calculations for entire iso-electronic sequences. This work represents the first of these *R*-matrix sequence calculations as part of the RmaX[2] effort whose aim is to study collisional processes important in astrophysical plasmas. Since an *R*-matrix calculation consists of several stages, it would be time consuming (and inefficient) to manually perform each step for every calculation in the sequence. Therefore, we have taken advantage of the robustness of the current suite of *R*-matrix codes and automated the entire calculation process. The automation allows each calculation to require less manpower but, more importantly, it ensures that each calculation is performed uniformly. We have also had to develop techniques to visualize the large amount of collisional data being produced by all of the calculations. This analysis is vital in ensuring the consistency of the results.

Performing calculations along the iso-electronic sequence is the natural choice when attempting to provide a large set of baseline atomic data. After choosing the target expansion, the details of the scattering calculation for each ion remain basically the same. It is also useful to examine the results along the iso-electronic sequence to investigate trends and look for errors in the data. These sequence calculations are intended to improve upon the current data available which consists of either distorted wave or plane-wave Born calculations. Of particular interest are the ions around shell boundaries. We are focusing on F-like ions in this work which are important for recombining and/or photoionized plasmas. With only a few exceptions, previous calculations for excitation of F-like systems were done using distorted wave or LS-coupling *R*-matrix theory. These calculations have been summarized in detail by Bhatia (1994). Extensive level-resolved *R*-matrix calculations have been previously performed for Ne^{+} (Griffin *et al* 1998) and Fe^{17+} (Witthoeft *et al* 2006). Calculations have also been performed for the $^2P_{3/2-1/2}$ fine-structure transition over the entire iso-electronic sequence from Ne^{+} to Ni^{19+} (Saraph and Tully 1994, Berrington *et al* 1998).

The rest of the paper will proceed as follows. In section 2, we will outline the calculation method. We will examine the structure of the F-like ions in section 3, comparing both our energies and radiative data with previous calculations and observations. In section 4, we will look at the results of the scattering calculations. Finally, we will summarize our findings in section 5.

2. Sequence calculations

The aim of this work is to perform *R*-matrix calculations using the intermediate-coupling frame transformation (ICFT) method (see Griffin *et al* (1998)) for all F-like ions from Ne^{+} to Kr^{27+}. The details of the calculation for each ion follow closely to those of the previous work on F-like Fe by Witthoeft *et al* (2006). In order to perform these calculations in a reasonable amount of time, we have scaled the size of the problem so that the calculation of a single ion takes around one day on our local cluster. To achieve this, we have chosen the following configuration basis set: $2s^2\ 2p^5$, $2s\ 2p^6$, $2s^2\ 2p^4\ 3l$, $2s\ 2p^5\ 3l$ and $2s^2\ 2p^4\ 4l$. This results in 87 LS terms and 195 IC levels. Over most of the sequence, we use 30 continuum basis orbitals per channel. At the low end of the sequence, however, this is increased (up to 50 continuum basis orbitals for Ne^{+}) to avoid oscillations in the high-energy collision strengths.

It is important to maintain consistency in the calculations along the iso-electronic sequence so that comparisons along the sequence reflect changes in the physics instead of numerical

[2] Web page: http://amdpp.phys.strath.ac.uk/UK_RmaX.

differences. For this reason, we have written a script (Whiteford and Witthoeft 2007) that will perform the entire *R*-matrix calculation, which involves a series of separate calculations, to ensure that the collision strengths for each ion are determined in a consistent manner. At the end of each run, the script produces a file containing Maxwell-averaged (effective) collision strengths in the adf04 format of ADAS (Summers 2004). Note that these effective collision strengths are tabulated, in the adf04 file, using the standard grid of 13 temperatures used by ADAS which ranges from $2 \times 10^2 (z+1)^2$ K to $2 \times 10^6 (z+1)^2$ K, where z is the residual charge of the ion (nuclear charge minus the number of electrons). The level of automation we use is possible (and reliable) because of the large effort undertaken over the last 15 years in making robust the suite of *R*-matrix codes that we are using for these calculations. As we increase the nuclear charge, Z, we must decrease the z-scaled energy-mesh spacing used in the outer region so that the resonance features are properly resolved. We use the following energy meshes (in z^2 Ry) over the sequence: 10^{-4} ($Z = 10$–15), 5×10^{-5} ($Z = 14$–22), 10^{-5} ($Z = 20$–30) and 5×10^{-6} ($Z = 28$–36). Note that some calculations are repeated for values of Z where the energy mesh is changed in order to check the convergence of the effective collision strengths with respect to resonance resolution. We also allow to change the Thomas–Fermi scaling parameters used in AUTOSTRUCTURE when obtaining the wavefunctions. This will be discussed in detail in the next section.

For most of the calculated sequence we expect the ICFT calculations to provide accurate results, however, at the upper end of our range, relativistic effects become increasingly important. Although the current calculations do include relativistic Breit–Pauli corrections perturbatively (mass–velocity, spin–orbit and Darwin terms), fully relativistic Dirac–Fock *R*-matrix calculations may be necessary to obtain accurate results for $Z \geqslant 34$. The current calculations for these ions will provide a useful comparison with future fully relativistic calculations.

For the near-neutral ions, *R*-matrix with pseudostates (Bartschat *et al* 1996) calculations are expected to give more accurate results. In addition to an improved structure, *R*-matrix with pseudostates (RMPS) calculations benefit from being able to represent ionization loss from the scattering process. The current calculations are again useful for comparisons with future RMPS calculations. We also repeat our calculations for the first four ions of the sequence where the target energies have been adjusted to match observed values (NIST v. 3). This is done as an attempt to improve the positions of the resonances. In table 1, we show the calculations performed for each energy mesh. The 'XX' marks where an additional calculation was performed using an adjusted-energy target.

3. Structure

The orbital basis functions used in the present calculations were calculated using AUTOSTRUCTURE (Badnell 1986) where the energies were optimized separately (but in an identical manner) for each ion along the sequence. To optimize the energies, the equally weighted sum of all LS term energies was minimized by adjusting the radial scaling parameters applied to each orbital. From $Z = 20$–36, the scaling parameters change only by a couple of per cent. However, they change from between 5 and 20% from $Z = 10$ to $Z = 20$ showing that there is much more sensitivity of the low-Z energy levels. The optimization procedure is done automatically in AUTOSTRUCTURE with no manual intervention. While manual adjustment can improve the energies further, it is important to maintain consistency so that comparisons across the sequence do not reflect arbitrary changes in the approach to the structure. However, as will be shown in section 4.2, this results in rather poor energies for the first couple of ions

Table 1. Calculations performed for each outer-region energy mesh. The mesh spacings are given at the top of the table in z^2 Ry where z is the residual charge of the ion ($z = Z - 9$ for F-like systems). Calculations performed using each energy mesh have been marked with an 'X', while 'XX' indicates that an additional, energy-adjusted calculation was also performed.

Z	1×10^{-4}	5×10^{-5}	1×10^{-5}	5×10^{-6}
10	XX			
11	XX			
12	XX			
13	XX			
14	X	X		
15	X	X		
16		X		
17		X		
18		X		
19		X		
20		X	X	
21		X	X	
22		X	X	
23			X	
24			X	
25			X	
26			X	
27			X	
28			X	X
29			X	X
30			X	X
31				X
32				X
33				X
34				X
35				X
36				X

in the sequence. Although we repeat the calculations for the first four ions using observed energies, calculations which include ionization loss are truly needed for these ions.

3.1. Energy levels

Due to the method of optimizing the energy levels, the $n = 3$ level energies show better agreement with observations than the two $n = 2$ excited levels. In figure 1 are the per cent differences over the entire iso-electronic sequence of the $n = 2$ excited levels and a 3s level with what is listed by NIST v. 3. We see that the energy of the fine-structure level is within 1% agreement of NIST only beyond $Z = 30$. The accuracy of the 2s $2p^6\ ^2S_{1/2}$ level is only marginally better. As we will see in section 4.3, although not very accurate in terms of spectroscopy, the accuracy of the $n = 2$ energy levels is sufficient for the scattering calculations to give results in good agreement with previous calculations for most of the ions ($Z > 13$). The agreement of the 3s level (which is representative of the rest of the excited levels) is within 1% of NIST after $Z = 15$. All level energies are poor for the first couple of ions.

As a final look at the energy levels, we show in figure 2 the distribution of the levels for selected ions along the sequence. The energies have been $1/z^2$-scaled, where $z = Z - 9$ for

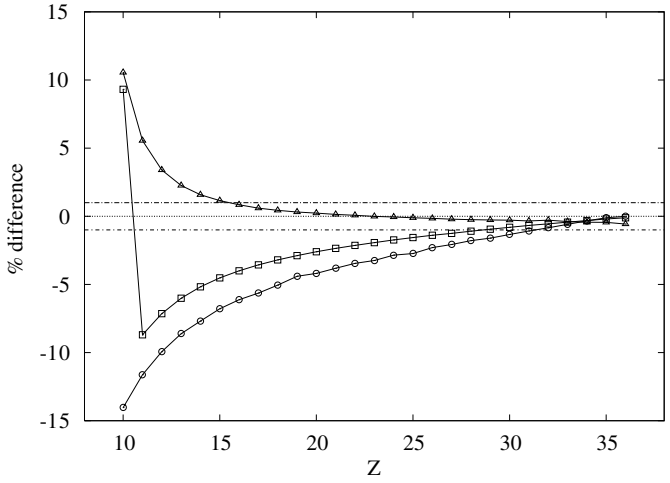

Figure 1. Per cent difference between the energy levels of the present calculations and the observed energies listed in NIST v. 3. The circles are for the $2s^2\ 2p^5\ ^2P_{1/2}$ fine-structure level, the squares are for the $2s\ 2p^6\ ^2S_{1/2}$ level and the triangles are for the $2s^2\ 2p^4\ 3s\ ^4P_{5/2}$ level. The dashed horizontal lines mark $\pm 1\%$.

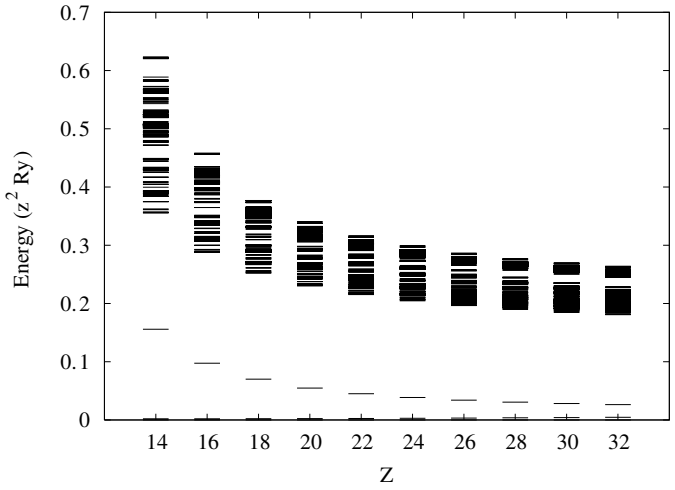

Figure 2. Energy levels in z^2 Ry (where z is the residual nuclear charge) for several ions along the sequence.

the F-like sequence. The most prominent feature of the figure is the widening gap between the $n = 4$ and $n = 3$ excited levels as the nuclear charge increases. Due to this large separation of the $n = 3$ and $n = 4$ levels at the upper end of the sequence, we would expect less mixing between these complexes.

3.2. Radiative data

As a further test of our structure, it is useful to compare radiative data (gf-values or A-values) with other calculations. Our main comparison is with the relativistic Hartree–Fock

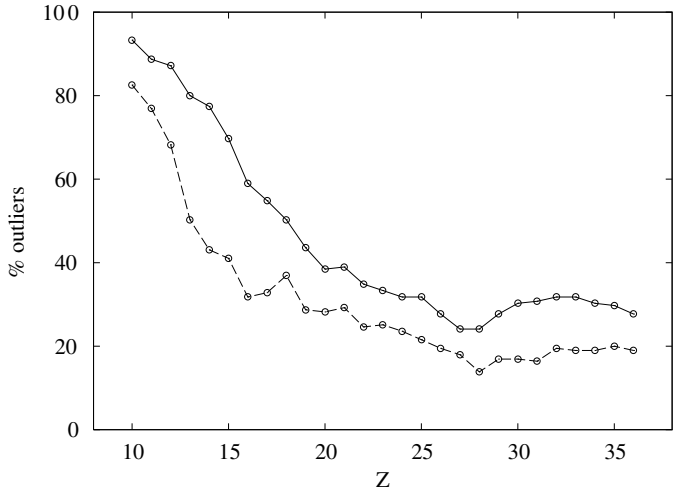

Figure 3. Percentage of transitions from the ground level where the length and velocity forms of the gf-value disagree by 20% (solid) and 50% (dashed).

calculations of Fawcett (1984) who obtained oscillator strengths for F-like ions from Mg^{3+} to Ni^{19+}. Their oscillator strengths can be considered reliable since they have optimized their results on observations. For Ne^{+}, we will compare our A-values with the multi-configuration Hartree–Fock calculation of Griffin *et al* (2001).

Before these comparisons, however, it is useful to check the agreement between the length and velocity forms of the gf-values for the present calculations. In figure 3, we show the percentage of transitions whose length- and velocity-form gf-values disagree by at least 20% and 50% for each Z. We see that, although poor for low-Z, the agreement improves rapidly along the sequence and levels off after $Z = 20$. However, there is still a sizeable fraction (30%) of transitions that still disagree by more than 20% for the most highly charged ions. The transitions which show the worst agreement are those with a small gf-value.

For the Ne^{+} calculation, we can compare the present A-values with the results of Griffin *et al* (2001). In figure 4, we show the ratios of the A-values from the Griffin *et al* results to those of the present calculation for transitions from the ground level to the $2s^2\ 2p^4\ 3s/3d$ levels. For this calculation, which has the worst structure of all the present calculations, we find that approximately 50% of the A-values agree within 10% of those in Griffin *et al*.

Next we compare our gf-values with the relativistic Hartree–Fock calculations by Fawcett (1984) for ions from Mg^{3+} to Ni^{19+}. Fawcett provides gf-values for transitions from both levels in the ground term to 3s and 3d levels for all ions in that range (with the exception of Co^{18+}) and also includes transitions among the $2s^2\ 2p^4\ 3l$ levels for Mg^{3+}, Al^{4+} and Si^{5+}. Again we compare our results by looking at the ratio of our gf-values (length form) with the results of Fawcett for each ion in Fawcett's compilation. These ratios are plotted against the magnitude of the gf-value for the present calculation in figure 5 for transitions to the 3s levels. The gf-value for the transition to the $^4P_{3/2}$ level is seen to change by more than an order of magnitude over the sequence while the gf-value for the transitions to the $^2P_{1/2}$ level hardly changes at all. For transitions with the largest gf-values, the agreement with Fawcett is at the 20% level. A similar comparison is made for transitions to the 3d ($J = 1/2$) levels in figure 6. Again, we find agreement with Fawcett roughly at the 20% level. There is very large

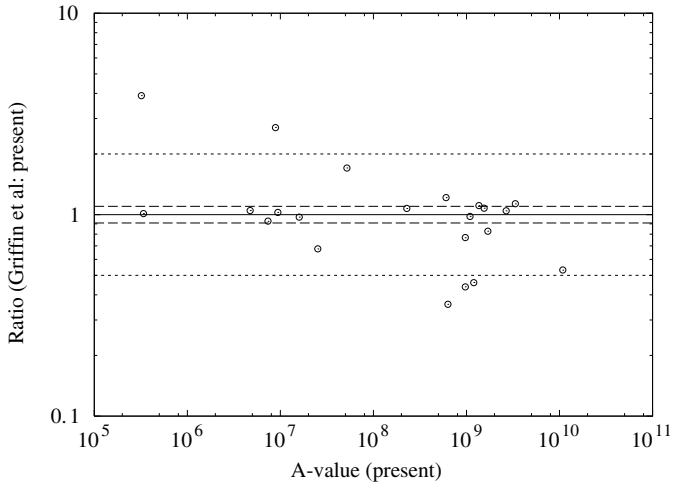

Figure 4. Scatter plot showing the ratio of the A-values from Griffin *et al* (2001) to the present results for transitions from the ground level to select 3s and 3d levels. The dashed and dotted horizontal lines mark agreement of 10% and a factor of 2, respectively.

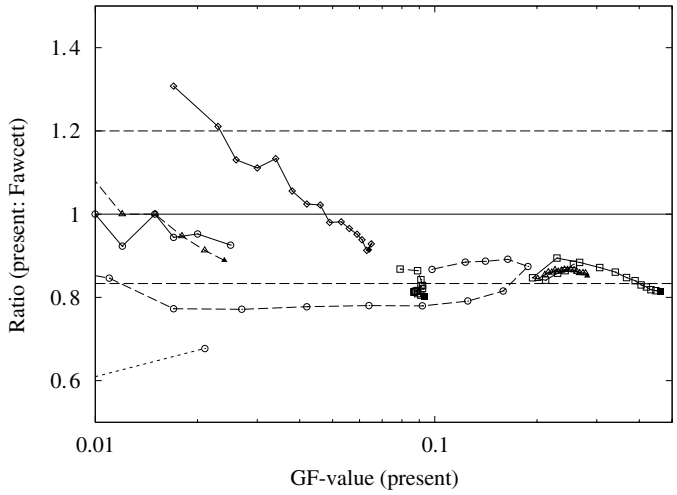

Figure 5. Comparison of gf-values from the present calculation to that of Fawcett (1984). Ratios of the gf-values are plotted versus the magnitude of the gf-value of the present calculation. The curves connect ratios along the iso-electronic sequence for each 3s transition from the ground level. The circles are ^{4}P terms (solid: $J = 5/2$, dashed: $J = 3/2$, dotted: $J = 1/2$), the squares are ^{2}P terms (solid: $J = 3/2$, dashed: $J = 1/2$), triangles are ^{2}D terms (solid: $J = 5/2$, dashed: $J = 3/2$) and the diamonds are for the $^2S_{1/2}$ level. The filled symbols mark the beginning of the sequence (in this case, Mg^{3+}). The dashed horizontal curves mark agreement at the 20% level.

disagreement between our gf-value and that of Fawcett for the transition to the $^2P_{1/2}$ level with $Z = 13$ (not visible in figure). This may be a tabulation error in the Fawcett paper since the rest of the gf-values for transitions to this level show much better agreement.

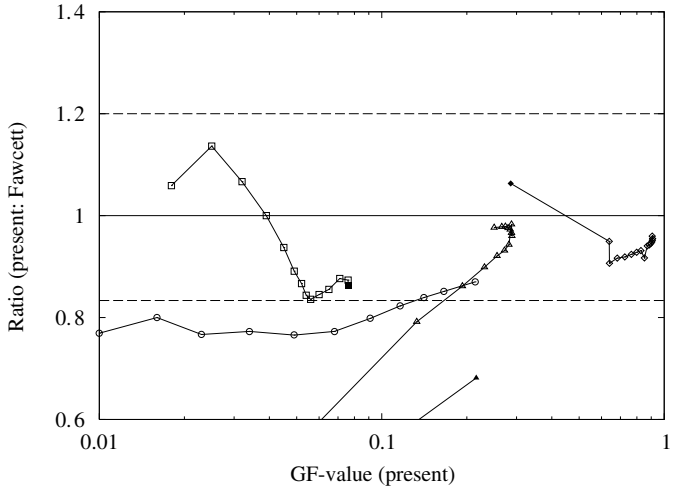

Figure 6. Same as figure 5 but for transitions from the ground level to the 3d $J = 1/2$ levels. Here, the circles show transitions to the $^4P_{1/2}$ level, squares and triangles mark different $^2P_{1/2}$ levels and the diamonds are transitions to the $^2S_{1/2}$ level.

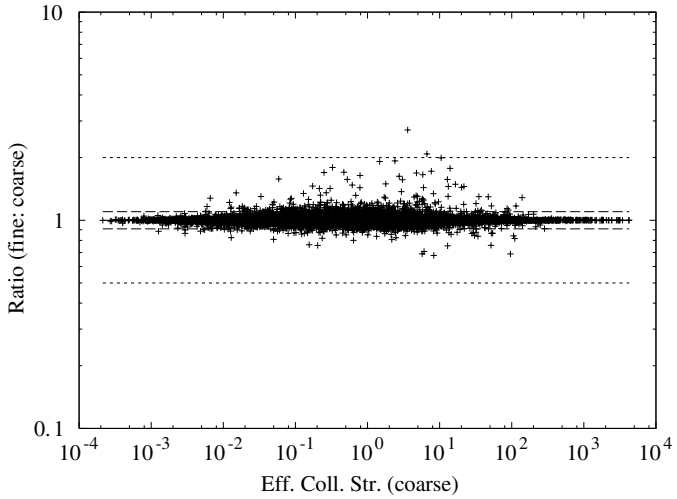

Figure 7. Scatter plot showing the ratio of effective collision strengths (at $T = 7.2 \times 10^4$ K) for the coarse- and fine-mesh calculations of Si^{5+}. The coarse mesh is $10^{-4}\,z^2$ Ry and the fine mesh is $5 \times 10^{-5}\,z^2$ Ry. The horizontal dashed lines mark agreement of 10% and the dotted lines denote agreement within a factor of 2.

4. Results and comparisons

4.1. Energy-mesh convergence

For ions along the sequence where the energy mesh is reduced, it is important to check that the resonances are sufficiently resolved by performing the calculation using both the fine and coarse meshes. The first overlap region where we change the mesh is from $10^{-4}\,z^2$ Ry to $5 \times 10^{-5}\,z^2$ Ry for Si^{5+} and P^{6+}. In figure 7, we show the ratio of the effective collision

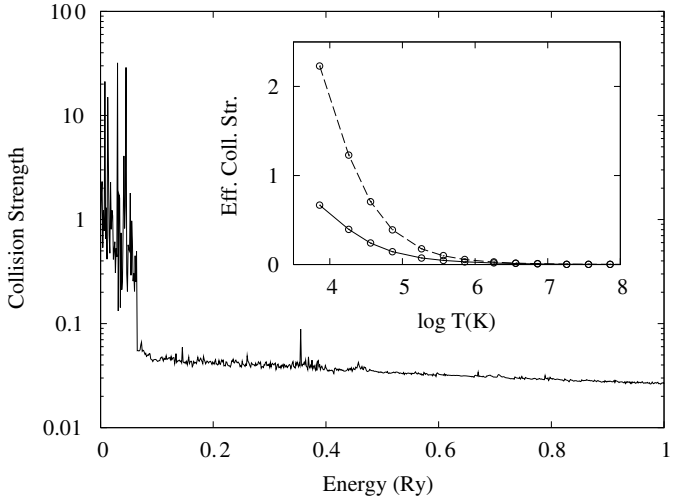

Figure 8. Collision strength of the $2s^2\ 2p^4\ 4d\ ^4D_{1/2}$–$^2P_{1/2}$ transition of Si^{5+} fine-mesh calculation. The inset shows the effective collision strength of the same transition for both the fine-mesh (solid) and coarse-mesh (dashed) calculations.

strengths from the fine-mesh calculation to the coarse-mesh calculation at a temperature of 7.2×10^4 K for Si^{5+}. These ratios are plotted against the magnitude of the coarse-mesh effective collision strength. This is a relatively low temperature where resonant enhancement of the effective collision strength is important and we see that there is very good agreement between the two calculations as a whole. Out of the 18 915 transitions, roughly 500 of them show disagreement by more than 10%. As the temperature increases, the agreement rapidly improves. The strongest and weakest transitions show excellent agreement since, in the case of the strong transitions, the background dominates the collision strength despite the presence of large resonances and, for the weak transitions, the resonances are almost non-existent. Therefore, the largest disagreement is usually seen for medium-strength transitions. The transition with the largest disagreement in figure 7 has a ratio of almost 3 and is the $2s^2\ 2p^4\ 4d\ ^4D_{1/2}$–$^2P_{1/2}$ transition. We plot the fine-mesh collision strength of this transition in figure 8. The inset of this figure shows a comparison of the effective collision strengths for both the fine- and coarse-mesh calculations. If plotted, the coarse-mesh collision strength would be almost indistinguishable from the fine-mesh calculation for the scale used here. The large differences between the fine- and coarse-mesh results for this transition are a result of insufficient sampling (see Badnell and Griffin (2001)) over the small energy range where the resonances are dominant ($E < 0.1$ Ry). For the majority of transitions, the magnitude of the resonances is more consistent over the resonance region which provides better sampling statistics in the effective collision strength convolution.

A useful way of quantifying the information in the scatter plot (but by losing information about the strength of the transition) is to count how many transitions disagree beyond a given percentage. In figure 9, we show the percentage of transitions that disagree by at least 10% and 20% when using the coarse and fine meshes for both Si^{5+} and P^{6+}. At the lowest temperature, there are a large number of transitions that show disagreement of more than 10% for both ions; however, less than 5% disagree by more than 20%. The agreement rapidly improves as the temperature is increased for both ions, and there is a clear improvement for the Si^{5+}

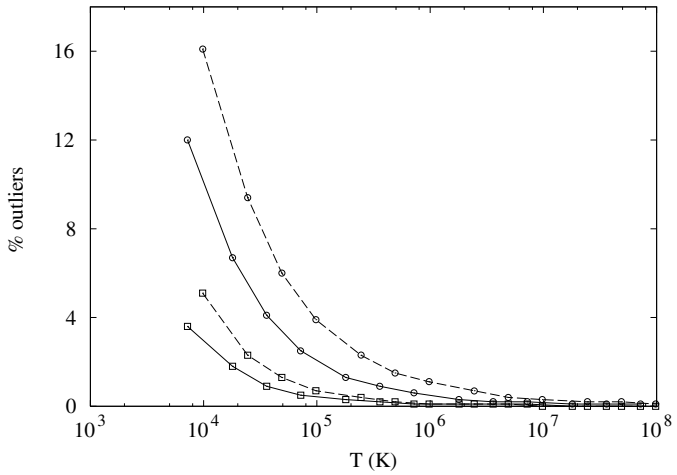

Figure 9. Percentage of all transitions whose effective collision strength disagrees by more than 10% (circles) and 20% (squares) when using a mesh of $10^{-4}\,z^2$ Ry versus $5 \times 10^{-5}\,z^2$ Ry. The solid curves are the results for the Si^{5+} calculations and the dashed curves show the results of the P^{6+} calculations.

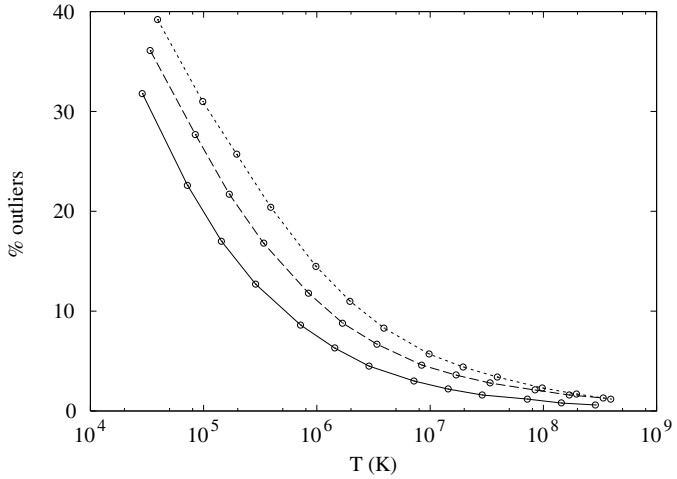

Figure 10. Percentage of all transitions whose effective collision strength disagrees by more than 10% when using a mesh of $5 \times 10^{-5}\,z^2$ Ry versus $10^{-5}\,z^2$ Ry. The three curves show the results for Ca^{11+} (solid), Sc^{12+} (dashed) and Ti^{22+} (dotted).

calculation over the P^{6+} calculation. The differences seen between the two ions are due to the narrower resonances present in the later calculation. Note that, since we have the fine-mesh results for both Si^{5+} and P^{6+}, we will only being using the results of the coarse mesh for the Al^{4+} calculation which we would expect to show even better agreement between fine- and coarse-mesh results.

The agreement between the fine- and coarse-mesh results is not as good when we switch from an energy mesh of $5 \times 10^{-5}\,z^2$ Ry to a mesh $10^{-5}\,z^2$ Ry. Calculations were performed using both of these meshes for Ca^{11+}, Sc^{12+} and Ti^{13+}. In figure 10, we show the percentage of outliers (for all transitions) beyond 10% agreement for these three ions as a function of

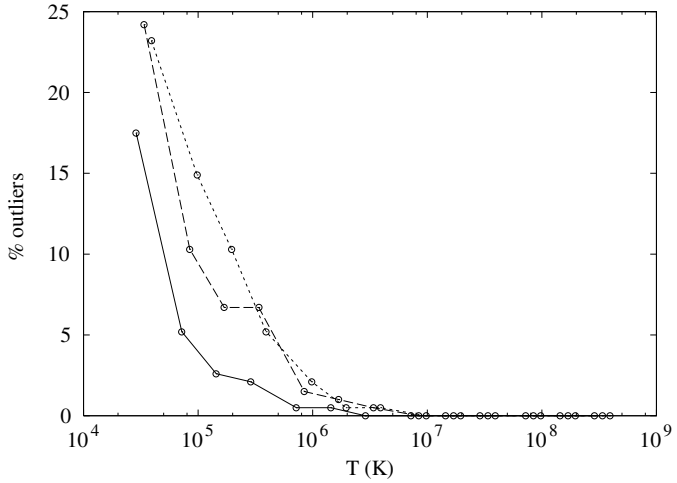

Figure 11. Percentage of transitions from the ground level whose effective collision strength disagrees by more than 10% when using a mesh of $5 \times 10^{-5}\, z^2$ Ry versus $10^{-5}\, z^2$ Ry. The three curves show the results for Ca^{11+} (solid), Sc^{12+} (dashed) and Ti^{22+} (dotted).

temperature. Although we still see that the number of outliers falls quickly with increasing temperatures, it is not as fast as is seen for the previous overlap region in figure 9. The total number of outliers is between 2 and 3 times greater than the previous overlap region. However, if we examine only transitions from the ground level, we see better agreement. In figure 11, we show this comparison. While there is still a large number of outliers at the lowest temperatures, the number drops very quickly with temperature. By the third tabulated temperature, the lowest Z ion (Ca^{11+}) shows the number of outliers to be less than 5% of the total number of transitions. Due to poorer statistics (since the curves in this figure represent far fewer transitions than in the last figure), the improvement with decreasing Z is not as uniform as seen when comparing the results from all transitions. Therefore, it is hard to say what the curve might look like for the previous ion in the sequence (K^{10+}), but we can be reasonably confident that it is at least as good as the Ca^{11+} results.

The last overlap region covers the Ni^{19+}, Cu^{20+} and Zn^{21+} calculations. A plot of the percentage of outliers over all transitions for this overlap region shows better agreement at the lowest four temperatures than the previous overlap region but is similar in magnitude over the rest of the tabulated range. We show the results for transitions from the ground level in figure 12. This plot is similar in shape to the analogous one for the previous overlap region but shows much better agreement overall, especially at the lowest temperatures. However, there is little improvement in the level of agreement as we move down the sequence (decreasing Z) as the curves for all three ions nearly lie on top of each other. This is also true when we look at the number of outliers coming from all transitions.

For low-density plasmas, such that exist for many astrophysical applications, it is the transitions from the ground level which are the most important. We find that, overall, the agreement for these transitions in the overlap regions is very good beyond $10^3(z+1)^2$ K. When examining all transitions, we only show good agreement beyond $10^4(z+1)^2$ K. Note that, if we are seeking agreement within 20%, the percentage of outliers decreases by approximately a factor of 2 in all cases. The effective collision strengths for transitions between excited levels are more uncertain due to structure, so improving the convergence of the resonances for

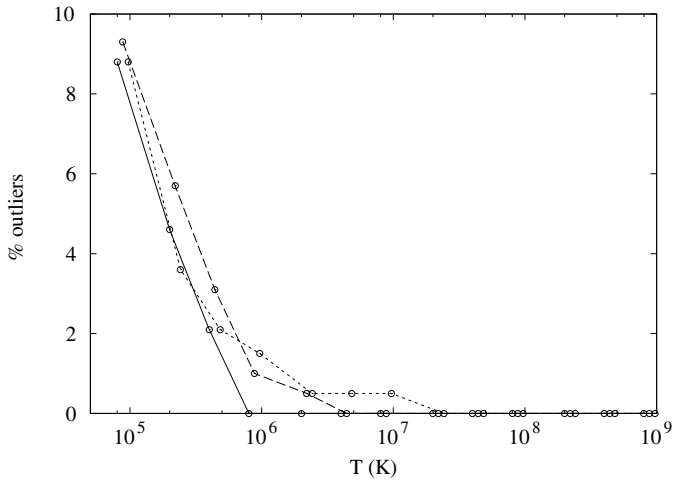

Figure 12. Percentage of transitions from the ground level whose effective collision strength disagrees by more than 10% when using a mesh of $10^{-5}\,z^2$ Ry versus $5 \times 10^{-6}\,z^2$ Ry. The three curves show the results for Ni^{19+} (solid), Cu^{20+} (dashed) and Zn^{21+} (dotted).

these transitions at low temperatures would do little to increase the confidence of the results without an equal improvement in the structure (of both energy levels and the size of the target expansion).

4.2. Adjusted-energy calculations

Typically, the energy levels of an *R*-matrix calculation are manually adjusted to match observed values as closely as possible. An accurate set of energy levels is not only needed to get an accurate background collision strength, but ensures that the complete set of resonances appear above the excitation threshold. A change in the resonance structure due to the adjustment of energy levels is the result of two things: (1) the direct modification of threshold energies and (2) levels can change energy order which introduces new resonance series into the collision strength. Since the structures for the first several ions in this sequence are poor, we have repeated the first four calculations ($Z = 10$–13) where the energies have been adjusted to match observed values. The energies of the $2l^5$, $2s^2\ 2p^4\ 3l$ and $2s^2\ 2p^4\ 4l$ configurations were adjusted while the $2s\ 2p^5\ 3l$ energies were left unchanged due to a lack of a near-complete set of observed energies from NIST for these ions. Although we are still lacking the representation of ionization loss that RMPS calculations include, we initially thought that these adjusted-energy calculations would give improved collision strengths over the unadjusted calculations. However, as discussed below, this turns out not to be the case for the near-neutral ions.

Comparing the adjusted-energy calculations with the unadjusted calculations, we find large differences at low temperatures while there is good agreement overall at high temperatures. Also, as we increase Z from 10 to 13, we find there is considerably better agreement between the unadjusted- and adjusted-energy results. While the adjustment of the resonance positions did have some effect, we find that, in many cases, it is the change of the background collision strength that causes the largest differences between the two calculations. Comparing with the *R*-matrix calculation of Griffin *et al* (2001) for Ne^+, we find that the adjusted-energy calculation is in worse agreement than the original, unadjusted calculation.

This leads us to believe that the shift of the background collision strengths, as a result of the energy adjustment, introduces an error in the results which is larger than the improvement in the resonance positions for this ion. Whether this is the result of the particularly poor energies levels for the Ne^+ calculation or is also the case when the energies are adjusted by smaller amounts is unclear. Due to their more accurate energies, we consider the results of Griffin *et al* to be more accurate than the present results. However, the Griffin *et al* results also do not represent ionization loss and calculations which do include this effect are needed for Ne^+, as well as $Z = 11$–13 where no other level-resolved *R*-matrix calculations exist to our knowledge. For the rest of the paper, reference to the present results is to the unadjusted-energy calculations.

4.3. Comparisons with previous calculations

Excitation calculations have been performed for a number of ions along the F-like iso-electronic sequence. Work before 1994 has been extensively reviewed by Bhatia (1994) which mainly consists of distorted wave and LS-coupling *R*-matrix calculations. Here, we will restrict ourselves to comparisons with previous level-resolved *R*-matrix calculations, which are few in number for the F-like sequence. The only comparison we can make along the entire sequence is for the $^2P_{3/2-1/2}$ fine-structure transition reported by Saraph and Tully (1994) and Berrington *et al* (1998). There are also two comprehensive *R*-matrix calculations we can use to compare transitions to, and between, excited levels. These are Griffin *et al* (2001) for Ne^+ and Witthoeft *et al* (2006) for Fe^{17+}.

As part of the IRON Project (Hummer 1993), two papers were published on the fine-structure transition along the F-like iso-electronic sequence. The first paper by Saraph and Tully (1994) covered ions with $Z = 10$–26 and was focused on the low-temperature effective collision strengths. To this end, they used a two-term model ($2s^2\ 2p^5\ ^2P$ and $2s\ 2p^6\ ^2S$) for their JAJOM *R*-matrix calculations. For some ions in the sequence ($Z = 18$, 22, 25 and 26), Saraph and Tully repeated their calculation where they adjusted the ^2S term energy to match observations. This adjustment was necessary in order to correctly position the resonances near threshold for these ions. The calculations of Saraph and Tully were then extended to high temperatures by Berrington *et al* (1998) who used a 28-term expansion which included the $2s^2\ 2p^4\ 3l$ configurations. Berrington *et al* also extended the sequence to include Co^{18+} and Ni^{19+}.

In figures 13 and 14, we show the effective collision strengths from the present calculations and Berrington *et al* as a function of nuclear charge at a temperature of 10^4 and $10^3\ (z+1)^2$ K, respectively. In the first figure, we see good agreement between the two calculations over the whole sequence. The ions that show the largest disagreement have $Z = 13$ and $Z = 17$–19 where we see differences on the order of 10–15%. For the ions where we used two different energy meshes to check the resonance resolution, there is excellent agreement between the fine-mesh and coarse-mesh results for this transition. Therefore, only the fine-mesh results are plotted in the figure.

At the lower temperature, in figure 14, we see periodic spikes of the effective collision strength as Z is increased. There are also larger differences between the present calculation and the results of Berrington *et al* at this temperature, particularly for values of Z where the spikes occur. These spikes in the effective collision strength are due to resonances which are shifted near to threshold as the nuclear charge is increased. Once the resonances move past threshold, they no longer contribute to the collision strength and we see a drop in the effective collision strength. Whereas both calculations agree to where the spikes occur, there are some large differences in the magnitude of the peaks, particularly at the lower charges. These low-temperature differences are aggravated by the poor structure of the first four ions

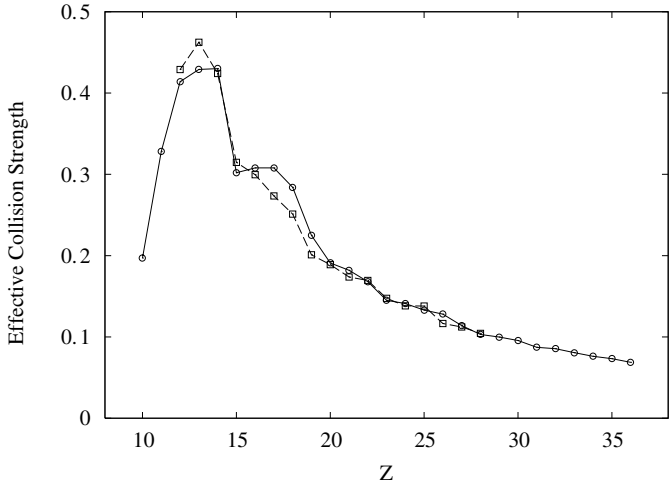

Figure 13. Effective collision strength of the fine-structure transition at a temperature of $T = 10^4\,(z+1)^2$ K along the iso-electronic sequence. The solid curve with circles is the present calculation and the dashed curve with squares is the result of Berrington *et al* (1998).

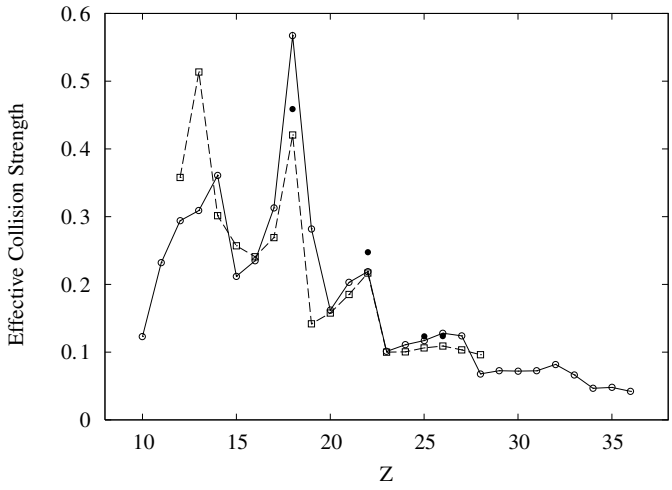

Figure 14. Effective collision strength of the fine-structure transition at a temperature of $T = 10^3\,(z+1)^2$ K along the iso-electronic sequence. The solid curve with circles is the present calculation and the dashed curve with squares is the result of Berrington *et al* (1998). The filled circles are the results from the adjusted-energy calculations of Saraph and Tully (1994).

in the sequence ($Z = 10$–13). For comparison, we also show, as filled circles in the figure, the adjusted-energy results of Saraph and Tully (1994). The unadjusted-energy results of Saraph and Tully agree very well with the results of Berrington *et al* and therefore are not shown. Of the four adjusted-energy calculations of Saraph and Tully, three of them agree better with the present results ($Z = 18, 25, 26$) than with Berrington *et al*. For $Z = 22$, the adjusted-energy results of Saraph and Tully are about 5% higher than the present results and the results of Berrington *et al*, which are in good agreement with each other.

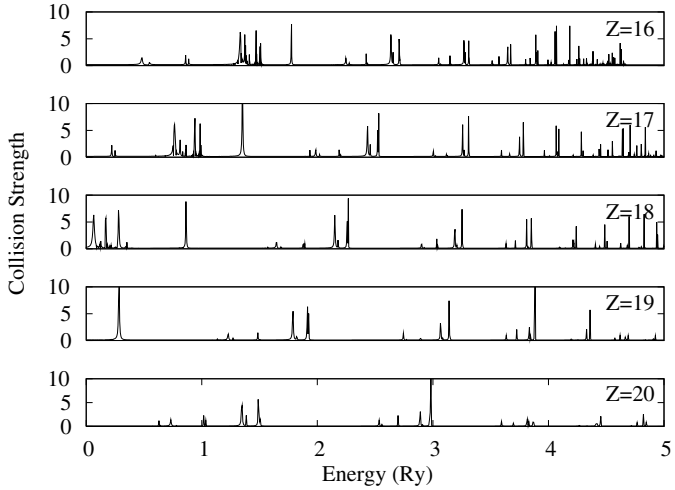

Figure 15. The march of the resonances: low-energy collision strengths for $Z = 16$–20.

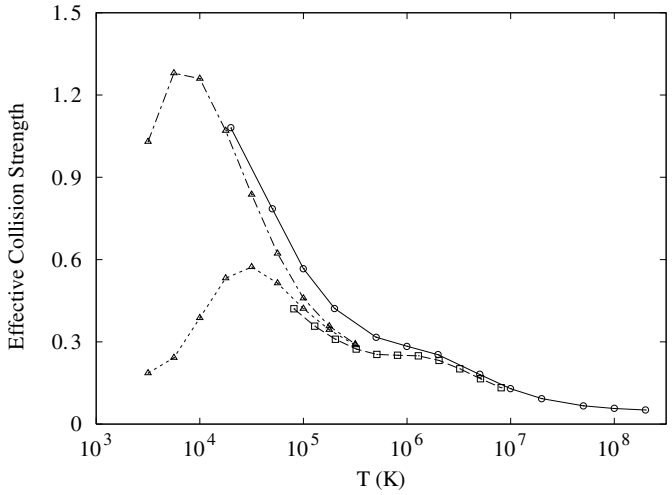

Figure 16. Comparison of the calculated fine-structure effective collision strengths for Ar^{9+}. The solid curve with circles is the present result, the dashed curve with squares is the result from Berrington *et al* (1998), the dotted curve with triangles and the dot-dashed curve with triangles are the unadjusted- and adjusted-energy results of Saraph and Tully (1994), respectively.

To demonstrate the cause of the peak structure in the low-temperature effective collision strengths, we plot the collision strengths for the ions around the peak at $Z = 18$ in figure 15. We can plainly see the group of resonances near $E = 1.3$ Ry for $Z = 16$ moving nearer to threshold as you increase the nuclear charge up to $Z = 18$. Afterwards, this group has moved past the threshold, which corresponds directly to the large peak in the effective collision strength seen in figure 14.

We examine more closely the fine-structure effective collision strength for Ar^{9+} in figure 16 where we compare the present results, the results of Berrington *et al*, and both the unadjusted-

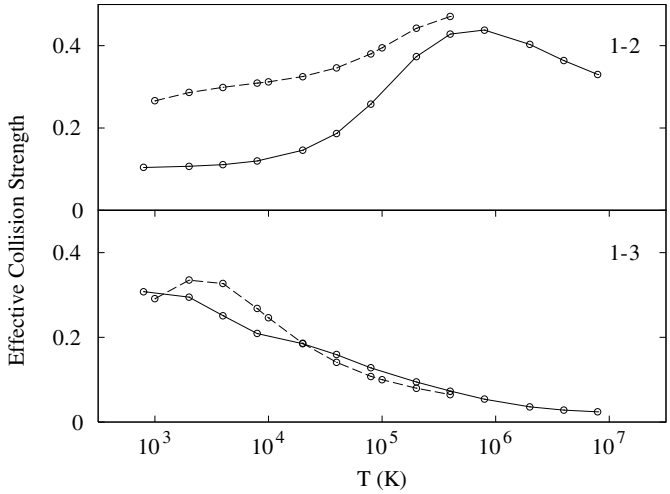

Figure 17. Effective collision strengths for the transitions from the ground level to the fine-structure level (1-2, top) and the $2s^2\ 2p^4\ 3s\ ^4P_{5/2}$ level (1-3, bottom). The solid curves are the present results and the dashed curves are the results from Griffin *et al* (2001).

and adjusted-energy results of Saraph and Tully. We see here that the energy adjustment makes a very large difference in the results of Saraph and Tully at low temperatures. The present results agree well with the adjusted-energy results of Saraph and Tully. The results of Berrington *et al* agree more closely with the unadjusted-energy results of Saraph and Tully which are significantly smaller at low temperatures for this ion.

The most extensive excitation calculation to date on Ne^+ was performed by Griffin *et al* (2001) using the ICFT *R*-matrix method. Although the current calculation has a larger target expansion (195 levels versus 138 levels), Griffin *et al* include pseudo-orbitals in their target calculations which allows them to have more accurate energies. Griffin *et al* calculate the fine-structure splitting in agreement with measurements and their higher excited state energies are shifted by approximately 0.05 Ry. For the current calculation, the fine-structure splitting disagrees with observations by almost 15% and the higher lying levels are shifted by around 0.2 Ry. We also note that, due to the different target expansions used in each calculation, a proper comparison of all transitions is nearly impossible, particularly between highly excited states. While levels can only be properly identified using total J, parity and the energy order, for this ion we find better agreement with the results of Griffin *et al* when we assume that the configuration and term labels are also good quantum numbers. Therefore, comparisons between the present calculation and the results of Griffin *et al* will be made using this mapping scheme.

In figure 17, we show the effective collision strengths for the transitions to the fine-structure level (top) and the $2s^2\ 2p^4\ 3s\ ^4P_{5/2}$ level (bottom). The solid curves show the present results and the dashed curves are the results from Griffin *et al*. For the fine-structure transition (1-2), we see that the present results are too low by about a factor of 2.5. However, there is better agreement near the peak of the effective collision strength. We see relatively good agreement, however, between the present results and those of Griffin *et al* for the transition to the $2s^2\ 2p^4\ 3s\ ^4P_{5/2}$ level. We show, in figure 18, the percentage of transitions from the present calculation which agree within 10%, 20%, 50% and 100% of the results of Griffin *et al*. Here, we see that the overall agreement between the two calculations is only weakly

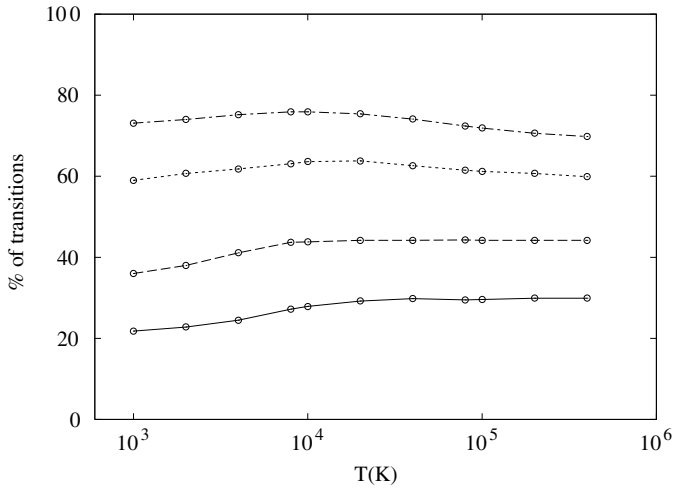

Figure 18. Percentage of transitions from the present Ne^+ calculation and Griffin *et al* (2001) which agree within 10% (solid), 20% (dashed), 50% (dotted) and 100% (dot-dashed).

Table 2. Configurations included in the previous $n = 3$ and $n = 4$ F-like Fe calculations of Witthoeft *et al* (2006) and the present calculation.

Configuration	$n = 3$	$n = 4$	Present
$2s^2\ 2p^5$	X	X	X
$2s\ 2p^6$	X	X	X
$2s^2\ 2p^4\ 3l$	X	X	X
$2s\ 2p^5\ 3l$	X	X	X
$2p^6\ 3l$	X	X	
$2s^2\ 2p^4\ 4l$		X	X
$2s\ 2p^5\ 4l$		X	
$2p^6\ 4l$		X	

affected by temperature. This indicates that, unlike the transition shown in the bottom of figure 17, most of the differences seen between the present calculations and Griffin *et al* are due to differences in the background rather than the resonant enhancement. Had resonances played a larger role, we would expect to see improved agreement as the temperature is increased.

The most comprehensive test of the new data for the highly charged ions is made for Fe^{17+} comparing against the recent *R*-matrix calculations of Witthoeft *et al* (2006). In the previous work, two calculations were made: one including only $n = 3$ configurations and the other using configurations up to $n = 4$. Significant differences were seen between the two calculations due to the effects of the $n = 4$ levels. In the present calculation, we attempted to include the $n = 4$ configurations which have the most impact on the $n = 3$ transitions without making the calculations too large. In table 2, we show the configurations included in the two previous calculations and the present calculation. Before looking at the general trends over all transitions, it is useful to look again at the fine-structure transition. In figure 19, we compare the present results with the two calculations in Witthoeft *et al* (2006) and the results of Saraph and Tully (1994) and Berrington *et al* (1998). The difference between the $n = 3$

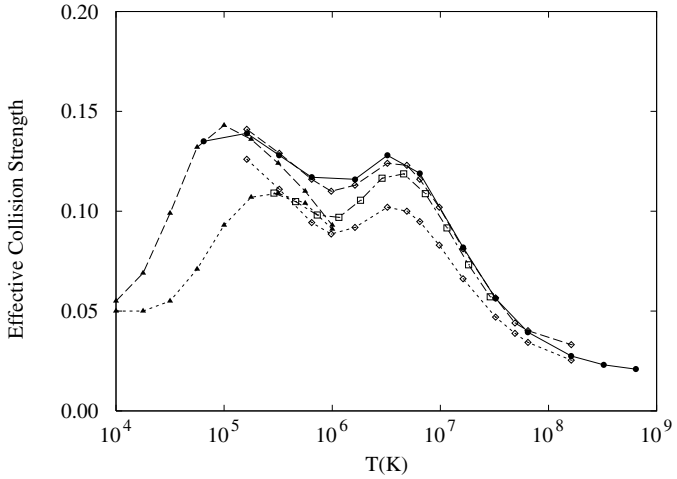

Figure 19. Comparison of effective collision strengths between many calculations for the fine-structure transition of Fe^{17+}. The solid curve with filled circles is the result from the present calculation, the dotted and dashed curves with open diamonds are the results from the $n = 3$ and $n = 4$ calculations from Witthoeft *et al* (2006), the dot-dashed curve with open squares is the result of Berrington *et al* (1998), and the dotted and dashed curves with filled triangles are the unadjusted- and adjusted-energy calculations of Saraph and Tully (1994).

and $n = 4$ calculations of Witthoeft *et al* is clearly seen and the present calculations agree very well with the larger $n = 4$ calculation. This indicates that we have included the most important $n = 4$ related structure in the present calculation, at least for this transition. We also see good agreement with Berrington *et al* at high temperatures. As with Ar^{9+}, Saraph and Tully calculated effective collision strengths for this ion using unadjusted- and adjusted-energy targets. As was the case before, the present results agree more closely with the adjusted-energy results while the Berrington *et al* calculation agrees well with the unadjusted-energy results at low temperature. Saraph and Tully also report results from a Breit–Pauli R-matrix calculation for this ion which agrees well with their adjusted-energy results.

It can be difficult to assess the agreement of all the transitions from the new Fe^{17+} calculation with the previous calculations of Witthoeft *et al*. Part of this difficulty is due to the large amount of data: nearly 20 000 transitions on a tabulated grid of 13 temperatures for the present calculation. However, the primary difficulty in the comparison, as was the case with Ne^+, comes from matching the levels from one calculation to another due to the different target expansion used in each calculation. For the results we show here, the matching was done by first considering only the set of levels from the same configuration set and then mapping according to the usual J, parity and energy order. As previously discussed, this does not lead to perfect matching; however, we can achieve a good match for the majority of levels. Furthermore, for those levels which we are unable to match using our method, we can identify the transitions where disagreement between two calculations is due to poor level matching instead of differences in the calculations. This identification is done by examining scatter plots of the ratio of effective collision strengths from two calculations, Υ_1/Υ_2, versus the magnitude of the effective collision strength, Υ_2. An example of this is given in figure 20 where we show the ratio of effective collision strengths from the previous $n = 4$ calculation (Υ_1) to the present calculation (Υ_2) at a temperature of 6.48×10^7 K. For the vast majority of the transitions, the agreement is within a factor of 2. However, there are many transitions

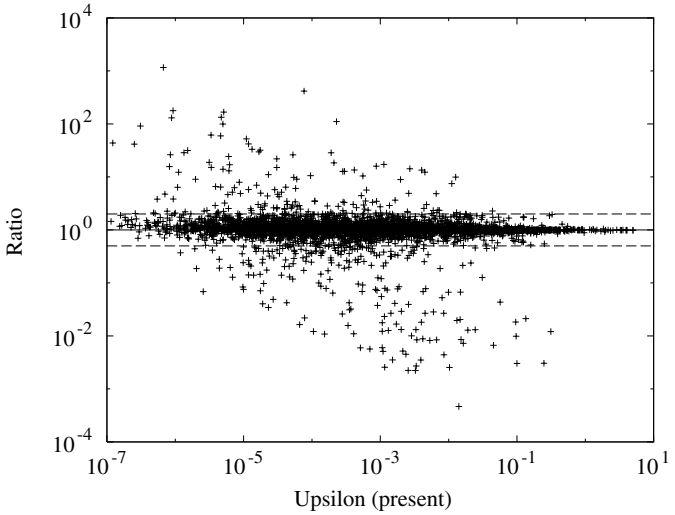

Figure 20. Ratios of effective collision strengths from the $n = 4$ calculation by Witthoeft *et al* (2006) compared to the present calculation for Fe^{17+}. The dashed horizontal lines mark agreement at a factor of 2.

where the disagreement is much larger. The collection of these points is spread from the upper left of the plot to the lower right. Due to the choice of axes, points distributed in this manner are characteristic of mismatching between the levels of these transitions. The level identifications for these transitions are either incorrect or there is simply not a common identification for them between the two calculations. This problem with level matching can have implications in plasma modelling where atomic data are taken from a variety of sources. It can be impossible to completely match the set of A-values from one calculation with collisional data from another, particularly for transitions to highly excited levels.

While figure 20 is very useful in seeing absolute differences between two calculations, it is also useful to see how the agreement between these calculations is affected by temperature. In figure 21, we show the percentage of transitions from the present calculation whose effective collision strengths disagree by more than 20% from the two previous calculations in Witthoeft *et al* (2006). We have limited the comparisons in this figure for strong transitions whose effective collision strength is greater than 10^{-2}. Each curve represents transitions between different configuration groups. Comparisons with the previous $n = 3$ and $n = 4$ calculations are marked with either open symbols ($n = 3$) or filled symbols ($n = 4$).

Looking first at transitions from the ground level, we can see that the results of the present calculations agree much better with those of the previous $n = 4$ calculation than with those of the $n = 3$ calculation. This indicates that the inclusion of the $2s^2\ 2p^4\ 4l$ levels in the target of the present calculation captures most of the important effects for these transitions. The comparison curve of the $n = 4$ calculation is flat with temperature which indicates that the main difference between the two calculations is with the background of the collision strength rather than the resonances. Examining the $n = 3$ comparison curve, we see that there is a very large number of transitions that disagree at low temperatures, but the agreement is noticeably better (although not as good as the $n = 4$ comparison) at higher temperatures. This additional, low-temperature disagreement is due to differences in the resonant enhancement of the two calculations while the amount of disagreement at high temperatures gives us an

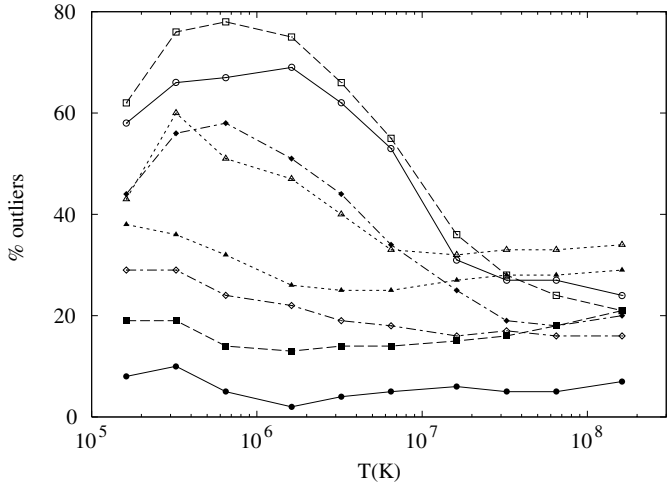

Figure 21. Per cent of transitions whose effective collision strengths between the present calculation and those from Witthoeft *et al* (2006) disagree by more than 20%. Only transitions with an effective collision strength (given by the present calculation) greater than 0.01 are considered. The solid curves with circles are for transitions from the ground level, the dashed curves with squares are for transitions between $2s^2\ 2p^4\ 3l$ levels, the dotted curves with triangles are for transitions from $2s^2\ 2p^4\ 3l$ levels to $2s\ 2p^5\ 3l$ levels and the dot-dashed curves with diamonds are for transitions between $2s\ 2p^5\ 3l$ levels. The open symbols are comparisons between the present calculations and the $n = 3$ calculation of Witthoeft *et al* and the filled symbols compare the present calculation with the previous $n = 4$ calculation.

indication of the level of agreement of the background collision strength for these transitions. Note that a fraction of the outliers are due to the mismatching of levels discussed above. Of these transitions from the ground level, the transitions to the $2s^2\ 2p^4\ 3l$ levels are in excellent agreement with the previous $n = 4$ calculation for all temperatures (we find disagreement $>10\%$ for only a couple of transitions). Comparisons for transitions to the $2s^2\ 2p^4\ 4l$ levels are more difficult. Several of these levels mix strongly with $2s\ 2p^5\ 4l$ levels in the previous $n = 4$ calculation. However, since we do not include those configurations in the present calculation, these highly mixed levels are not truly comparable. Disregarding transitions to these levels, we see good agreement between the old $n = 4$ calculation and the present calculation at the peak-abundance temperature for collisionally dominated plasmas (Mazzotta *et al* 1998).

We see similar features when looking at the comparison for transitions between $2s^2\ 2p^4\ 3l$ levels. Here, we find that 20% of the transitions have effective collision strengths which consistently disagree by more than 20% at all temperatures (compared to 10% for the transitions from the ground level). We also see the same behaviour with temperature for the comparison curve for the $n = 3$ calculation. There is worse agreement between the results of the present calculation and those from both previous calculations for transitions between the $2s^2\ 2p^4\ 3l$ levels and the $2s\ 2p^5\ 3l$ levels, although there is still slightly better agreement with the $n = 4$ calculation. There is an indication that we are missing some resonant enhancement in the present calculations for these transitions since there is a little more variation of the $n = 4$ comparison curve with temperature. Most of these differences come from the weaker transitions and there appears to be significant mapping problems for these transitions which makes a true comparison difficult.

Finally, we consider the curves for transitions between the 2s $2p^5$ $3l$ levels. Here, the present calculations agree much more closely with the $n = 3$ calculation at low temperatures. At high temperatures, we find that about 20% of the transitions disagree with both the previous calculations. Here, we conclude that it is necessary to include the other $n = 4$ configurations to accurately determine the effective collision strengths for these transitions.

We can conclude a number of things from these comparisons with Fe^{17+}, which can extend to other nearby ions. For transitions from the ground level we see good agreement with the previous $n = 4$ calculation. While there is still some uncertainty in the low-temperature effective collision strengths, we can be confident in the present results beyond $2 \times 10^3 (z+1)^2$ K, which is well below the peak-abundance temperature for collisionally dominated plasmas (Mazzotta *et al* 1998). There is greater uncertainty for transitions between the excited levels, particularly at low temperatures; however, many of these differences are the result of difficulties in mapping the levels from the different calculations. For transitions between $2s^2$ $2p^4$ $3l$ levels, we see fairly good agreement with the previous $n = 4$ calculation of Witthoeft *et al* (2006) over the entire temperature range. For the strongest transitions, we see good agreement between all three calculations. As a whole, we can be confident that the present results are an improvement over a similar-sized distorted wave calculation. More work needs to be done to see how the present calculations fare at the upper end of the sequence where relativistic effects, beyond a perturbative treatment, are important.

4.4. Iso-electronic trends

The present set of *R*-matrix calculations provides a opportunity to examine how the effective collision strengths with resonant enhancement change over an iso-electronic sequence. In particular, we are interested in the effect that resonances have on the scaling of the effective collision strengths. Looking at the high-temperature effective collision strengths over the sequence, where they should vary smoothly, is useful in detecting possible errors in any one calculation. We are also interested in the possibility of interpolating the results from a subset of the sequence to obtain the effective collision strengths over the whole range for future sequences.

We first looked at the effective collision strengths across the iso-electronic sequence in figures 13 and 14 for the fine-structure transition. Here, we saw that the shifting of resonances near to threshold as Z increased caused large spikes in the low-temperature effective collision strength (figure 14). At slightly higher temperatures, however, we found that these spikes had largely disappeared. At even higher temperatures, beyond the resonance region, the effective collision strength for this transition varies smoothly with Z.

For levels where there is little mixing, the high-temperature effective collision strengths have a simple relationship with Z (as in figure 13). However, for many of the transitions, level mixing can cause the effective collision strength to exhibit complicated behaviour over Z. In figure 22, we show the transition from the ground level to the 4th $J = 3/2$ odd level (which is identified as the $2s^2$ $2p^4$ 3p $^2P_{3/2}$ level in the Fe^{17+} calculation). In the top panel of the figure is the effective collision strength (scaled as $(z+1)^2$) as a function of Z and in the bottom of the figure is the corresponding contribution of the term coupling coefficients (TCCs) for the excited level. For this excited level, there are three dominant terms over the calculated range of Z (note that there are other terms not displayed in the figure which do not contribute significantly). We can clearly see how the level mixing directly affects the effective collision strength.

As we examine transitions to the higher excited states, we find that the behaviour of the effective collision strength is not always smooth over Z when considering levels with the same

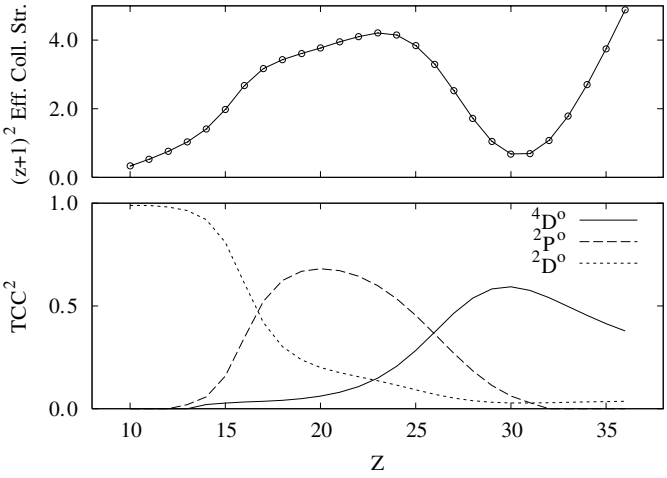

Figure 22. Effective collision strength of the 4th $J = 3/2$ odd level (labelled as $2s^2\ 2p^4\ 3p\ ^2P_{3/2}$ for F-like Fe) as a function of Z (top panel) and the corresponding dominant term coupling coefficients (TCCs) (bottom panel).

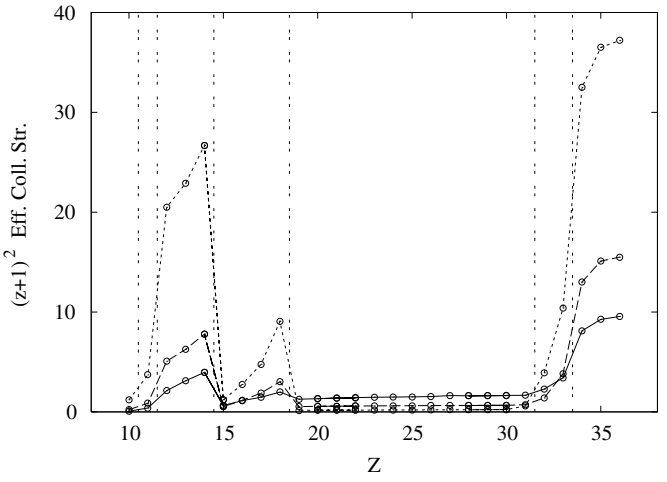

Figure 23. Effective collision strengths of the 17th $J = 5/2$ even level (labelled as $2s^2\ 2p^4\ 4d\ ^4D_{5/2}$ for F-like Fe) as a function of Z at three temperatures: 2×10^3, 5×10^4 and 1×10^6 $(z+1)^2$ K. The vertical lines mark where the configuration and term labels change.

J, parity and energy order. For these levels, we need to treat the configuration and term as good quantum numbers. An example of this is shown in figures 23 and 24. In the first figure are shown the effective collision strengths for the transition from the ground level to the 17th $J = 5/2$ even level at three temperatures: $2 \times 10^3, 5 \times 10^4$ and $1 \times 10^6\ (z + 1)^2$ K. The vertical lines in the figure mark where the configuration and term designation for this level change. As we can see, the effective collision strength is discontinuous at precisely the points where the level identification changes. This behaviour indicates that there are effective level crossings among these $J = 5/2$ even levels. If we use the configuration and term as good

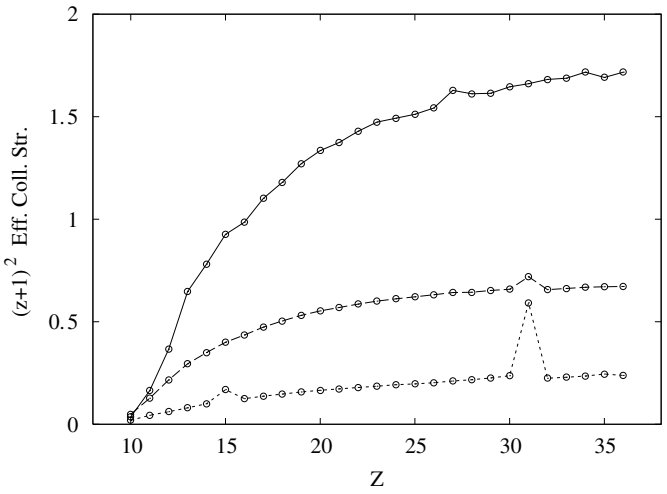

Figure 24. Effective collision strengths of the $2s^2\ 2p^4\ 4d\ {}^4D_{5/2}$ level as a function of Z at three temperatures: 2×10^3, 5×10^4 and $1 \times 10^6\ (z+1)^2$ K.

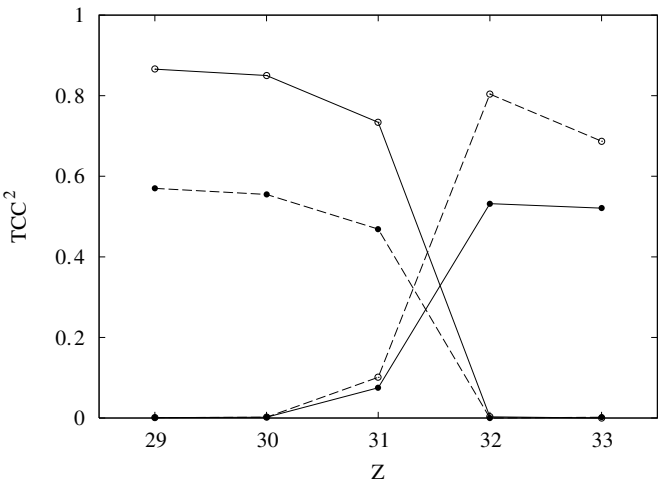

Figure 25. Dominant term coupling coefficients (TCCs) for the 16th (open circles) and 17th (filled circles) $J = 5/2$ even level for $Z = 29$–33. The solid curve represents the term coupling coefficient of the $2s^2\ 2p^4\ 4s\ {}^2D$ term and the dashed curve is for the $2s^2\ 2p^4\ 4d\ {}^4D$ term.

quantum numbers while ignoring the energy order, as shown in figure 24, we see that the effective collision strength varies smoothly over the entire range except for a couple of values of Z. The small fluctuations of the effective collision strength of the low-temperature curve are due to differences in the resonance structure. However, for $Z = 15$ and 31, we see that the high-temperature effective collision strength deviates significantly from the behaviour from the rest of the ions. These deviations are caused by level mixing at the point of level crossing. In figure 25, we show the square of the term coupling coefficients of the $2s^2\ 2p^4\ 4s\ {}^2D$ and $2s^2\ 2p^4\ 4d\ {}^4D$ terms for the 16th and 17th $J = 5/2$ even levels. Here, we see that the 16th

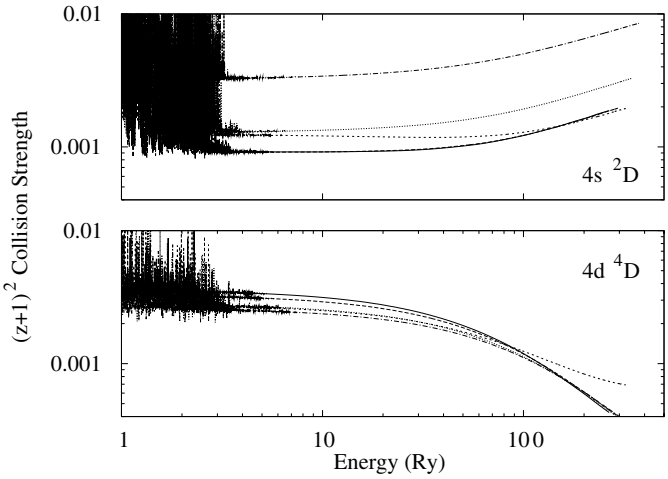

Figure 26. Collision strengths from the ground level to the 16th and 17th $J = 5/2$ even levels which are dominated by the $2s^2\ 2p^4\ 4s\ ^2D$ term (top panel) and the $2s^2\ 2p^4\ 4d\ ^4D$ term (bottom panel). The solid curve is for $Z = 31$ while the other curves represent the adjacent ions: $Z = 29$ (dashed), $Z = 30$ (dotted), $Z = 32$ (dot-dashed) and $Z = 33$ (dot-dot-dashed).

$J = 5/2$ even level switches from being dominated by the 4s ^{2}D term at $Z = 31$ to the 4d ^{4}D term at $Z = 32$. The 17th $J = 5/2$ even level has the opposite behaviour. At $Z = 31$, the level crossing is incomplete; that is, the levels have some contribution from both terms while, for the adjacent ions, there is no mixing between these terms. We show the effect of this mixing on the collision strengths in figure 26. In the top panel, we show the collision strength for the transition to the level (either 16th or 17th $J = 5/2$ even level) which is dominated by the 4s ^{2}D term for $Z = 29$–33 while the bottom panel shows the collision strength for the transitions to the level dominated by the 4d ^{4}D term. For all of the ions with $Z \neq 31$, we see a common high-energy behaviour; in the top panel the collision strength increases with energy, and in the bottom panel the collision strength decreases. For $Z = 31$, however, the mixing of the transition dominated by upward trending 4s ^{2}D term is affected by the downward trending 4d ^{4}D term and vice versa. The spike of the high-temperature effective collision strength at $Z = 31$ in figure 24 corresponds directly with the disparity between the high-energy collision strengths for $Z = 31$ and the adjacent ions in the bottom panel of figure 26. Although the high-energy effective collision strengths can be interpolated across Z for most transitions, interpolation for some transitions will be unreliable due to level mixing.

5. Summary

We have performed 195-level ICFT R-matrix calculations over the F-like iso-electronic sequence from Ne^+ to Kr^{27+}. At the low end of the sequence ($Z = 10$–12), poor structure increases the uncertainty of our calculations, however the comparison with the Griffin *et al* (2001) provides a bound of our uncertainty. For these ions, R-matrix with pseudostates (RMPS) calculations is more appropriate since ionization loss is important to consider in the excitation of near-neutral ions. The current results will be useful for comparisons with future RMPS calculations for these ions. Similarly, fully relativistic calculations may be required for the upper end of the sequence ($Z = 34$–36). We can find no other published

calculations to compare against (relativistic or otherwise) for these highly ionized species. For the rest of the sequence ($Z = 13$–33), the present calculations yield useful atomic data for transitions from the ground level (beyond $2 \times 10^3\ (z+1)^2$ K) and transitions between the $2s^2\ 2p^4\ 3l$ excited states (beyond $2 \times 10^4\ (z+1)^2$ K). Since the present calculations do not include the $2s\ 2p^5\ 4l$ levels, transitions to, and between, the $2s\ 2p^5\ 3l$ and $2s^2\ 2p^4\ 4l$ levels are more uncertain due to incomplete resonant enhancement. The present data for these transitions, however, still represent an improvement over distorted wave calculations which have no resonant enhancement at all. Not only do we find that resonance effects cause interesting behaviour of the effective collision strengths at low temperatures, but level mixing can lead to interesting structure of the effective collision strengths across the sequence at high temperatures where the resonances play no role. These data are made available in a number of databases (e.g. ADAS and CHIANTI). Future sequence work will concentrate on ions near shell boundaries, specifically the H-, He- and Li-like sequences as well as the Ne- and Na-like sequences.

Acknowledgments

This work has been funded by PPARC grant PPA/G/S2003/00055 and by the ADAS Project. Computational resources were funded by an EPSRC JREI award.

References

Badnell N R 1986 *J. Phys. B: At. Mol. Opt. Phys.* **19** 3827
Badnell N R and Griffin D C 2001 *J. Phys. B: At. Mol. Opt. Phys.* **34** 681
Ballance C P and Griffin D C 2004 *J. Phys. B: At. Mol. Opt. Phys.* **37** 2943
Bartschat K, Hudson E T, Scott M P, Burke P G and Burke V M 1996 *J. Phys. B: At. Mol. Opt. Phys.* **29** 115
Berrington K A, Saraph H E and Tully J A 1998 *Astron. Astrophys. Suppl.* **129** 161
Bhatia A K 1994 *At. Data Nucl. Data Tables* **57** 253
CHIANTI web page: http://www.chianti.rl.ac.uk
Fawcett B C 1984 *At. Data Nucl. Data Tables* **31** 495
Gorczyca T W, Pindzola M S, Shieh F S and McCreary C L 1995 *Comput. Phys. Commun.* **88** 211
Griffin D C, Badnell N R and Pindzola M S 1998 *J. Phys. B: At. Mol. Opt. Phys.* **31** 3713
Griffin D C, Mitnik D M and Badnell N R 2001 *J. Phys. B: At. Mol. Opt. Phys.* **34** 4401
Hummer D G, Berrington K A, Eissner W, Pradhan A K, Saraph H E and Tully J A 1993 *Astron. Astrophys.* **279** 298
Mazzotta P, Mazzitelli G, Colafrancesco S and Vittorio N 1998 *Astron. Astrophys. Suppl.* **133** 403
Mitnik D M, Pindzola M S, Griffin D C and Badnell N R 1999 *J. Phys. B: At. Mol. Opt. Phys.* **32** L479
NIST web page: http://physics.nist.gov/PhysRevData/ASD
Saraph H E and Tully J A 1994 *Astron. Astrophys.* **107** 29
Summers H P 2004 *The ADAS User Manual* version 2.6 (http://adas.phys.strath.ac.uk)
Whiteford A D and Witthoeft M C *ADAS8#3 User Guide* Available from http://adas.phys.strath.ac.uk
Witthoeft M C, Badnell N R, Del Zanna G, Berrington K A and Pelan J C 2006 *Astron. Astrophys.* **446** 361